Adaptive Robust Sliding-Mode Control of a Semi-active Seat Suspension Featuring a Variable Inertance-Variable Damping Device

Guangrui Luan, Pengfei Liu$^{(\boxtimes)}$, Donghong Ning$^{(\boxtimes)}$, and Guijie Liu

Ocean University of China, Qingdao 266000, China
{liupengfei,ningdonghong}@ouc.edu.cn

Abstract. This article introduces a novel mechanical variable inertance-variable damping (VIVD) seat suspension based on an adaptive robust sliding-mode (ARSM) controller, including its characteristics validation and performance experiment. In this paper, a variable damping (VD) device and a flywheel are connected in series to form a variable inertance (VI) device with real-time controllable inertance, which is connected in parallel with another VD device to form a VIVD device. A two-layer control scheme is proposed where an upper desired controller is designed based on adaptive robust sliding-mode control and the desired control force is calculated; then a force tracking control strategy with energy priority storage (EPS) is designed as the lower layer controller. Under road random excitation, the VIVD seat suspension exhibits 21.89% and 9.56% lower RMS acceleration values compared to the passive seat suspension and a semi-active traditional sliding-mode control seat suspension. The new system demonstrates advantages in controllability and energy efficiency, with energy consumption falling within the milliwatt range. The proposed semi-active VIVD device shows potential in vehicle vibration control.

Keywords: Variable inertance-variable damping · Seat suspension · Adaptive robust sliding-mode · Two-layer control scheme · Energy priority storage

1 Introduction

Commercial heavy-duty vehicles play an essential role in the logistics and transport industry. When working the driver of a heavy vehicle is subjected to severe vibrations from rough road and the vehicle's powertrain, suffering from the injuries causing low back pain [1]. The seat suspension is in direct contact with the human body, its vibration isolation performance impacts on human comfort, thus, research into various types of seat suspension is conducted in the field of vehicle vibration control [2].

Generally, the seat suspensions are classified as passive [3], semi-active [4] and active suspensions [5]. Compared to passive seat suspensions, semi-active seat suspensions are controllable with a fast response for different vibration conditions. Moreover, they possess the advantages of a simpler mechanical structure, less power consumption and fail-safe characteristics compared with active suspensions. The semi-active system

includes the variable damping (VD) device [6],variable stiffness (VS) device [7], and variable inertance (VI) device [8]. The inertance is characteristic of the inerter, which is a two terminals mechanical element corresponding to the spring and damper [13]. The force produced by an inerter is the inertance multiplied by the relative acceleration of the two ends [14], similar to the force produced by a spring is the stiffness multiplied by the relative displacement of the two ends. Ning et al. verified that a VD device and passive inerter can form mechanical networks with specific topologies, the magnetorheological fluid damper [15] and electromagnetic damper (EMD) [16] are utilized to design the novel VI device. After that, the semi-active variable equivalent stiffness and inertance (VESI) device implemented by an electrical network is proposed to improve the vibration reduction performance at both vertical and roll directions [17]. This paper proposed a VI device structure with a passive inerter and a electromagnetic variable damping device in serial, and validated its mechanical properties that are different from those of VD devices.

Besides the innovation in mechanical structure, there are also considerable researches on control strategies for semi-active systems. The adaptive fuzzy sliding-mode controller, H ∞ controller [18], direct voltage controller based on TS fuzzy model [19], Lyapunov type robust controller [20] etc. are used for the control of semi-active magnetorheological (MR) seat suspension. Hu et al. utilized a suboptimal control law, called steepest gradient control in the semi-active damper for the control, meanwhile, low-order admittance networks are employed in the passive parts to optimize the low-order positive real admittance functions [21]. By utilizing the mechanical properties variability with advanced control strategies, the vibration of the suspension is attenuated to a large extent.

This paper proposes a novel semi-active VIVD device structure and a two-layer control scheme. The upper controller is an adaptive robust sliding-mode controller that calculates the desired values. The lower controller ensures that vibration energy can be stored in the VI device, prioritising the use of this energy for vibration suppression. The key advantages of the proposed device and its controller are listed as:

1. The two mechanical properties, damping and inertance, can be independently validated and controlled.
2. A new ARSM controller and semi-active tracking control strategy are designed for VIVD seat suspension control.

The remaining sections of the paper are structured as follows: Sect. 2 presents a model and prototype of the VIVD seat suspension, which is then the subject of analysis and validation. The ARSM controller and force tracking performance of the VIVD device is discussed in Sect. 3; Sect. 4 shows the vibration control performance of the VIVD seat suspension. Finally, Sect. 5 presents the conclusions of this research.

2   VIVD Seat Suspension

2.1   VIVD Seat Suspension Model

A VI device can be created by serially connecting a VD device and a mechanical inerter. In [11], a flywheel is utilized as a mechanical inerter, connected in series with the VD unit to constitute a mechanical VI device. Moreover, the VD device exhibits efficient vibration

suppression at higher excitation frequencies. Theoretically, by parallelly connecting VD and VI devices and implementing a suitable control strategy, vibration reduction can be achieved across a broader excitation range.
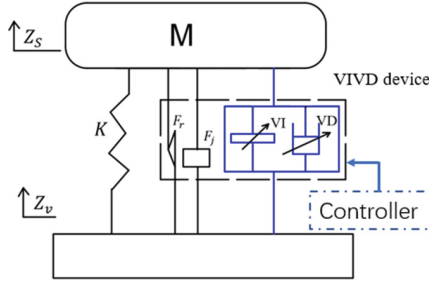

Fig. 1. The model of the VIVD seat suspension

This paper proposes a mechanical VIVD device that replaces the passive dampers in the seat suspension for vibration control. When VIVD devices are used in seat suspensions, the inherent inertance of the device and the friction between the components must be considered. Therefore, a simplified model of the VIVD seat suspension is illustrated in Fig. 1

$$m\ddot{Z}_s = -K(Z_s - Z_v) - F_{out} \tag{1}$$

$$F_{out} = F_r + F_j + F_{VD} + F_{VI} \tag{2}$$

where Z_s and Z_v are the displacement of the seat and cab chassis, K is the stiffness of seat suspension, F_r and F_j are the friction force and inherent inertance force of the VIVD device. F_{VD} is the output force of VD device, The damping and inertance of the VIVD can be controlled by the controller.

2.2 VIVD Device Prototype

In this article a prototype of the VIVD device is designed. Figure 2 Depicts the prototype of VIVD device. The orange section represents the motions of the VIVD device, since both the VD and the VI device are mounted between the seat and the cab chassis, the relative displacement is denoted as $Z_s - Z_v$, The ball screws are employed to transform the reciprocating motion of the seat suspension into a rotary motion represented by α,

$$\alpha = r(Z_s - Z_v) \tag{3}$$

$$r = 2\pi/d \tag{4}$$

where r is the transmission ratio of the ball screw, d is the lead of the ball screw, the $d = 0.032\,m$ in this design, and α is ration angle of the ball screw.

The VI and VD device both employ the permanent magnet synchronous motors (PMSM) as the damping adjustment device, the C_{vd} and C_{vi} are the damping generated by the PMSM. The shaft of the PMSM is connected with the ball screw, thus, the α is the ration angle of shaft. In the VD device, the PMSM directly is connected with the shell, which is mounted on the bottom of the seat. The force F_{vd} generated by VD device is:

$$F_{vd} = rC_{vd}\dot{\alpha} + F_{jvd} + F_{rvd} \qquad (5)$$

where $\dot{\alpha}$ is the rotational speed of the ball screw. F_{jvd} and F_{rvd} are the inherent inertance and the friction force generated by the VD device.

(a). VI device   (b). VD device

Fig. 2. The prototype of the VIVD device (a). VD device (b). VI device

However, in the VI device, the PMSM is not connected with "ground", the PMSM is connected to the flywheel and the two are rotated together, β is the ration angle of the flywheel. The relative rotational speed of ball screw and flywheel generates the output force F_{VI} of the VI device.

$$F_{vi} = rC_{vi}(\dot{\alpha} - \dot{\beta}) + F_{jvi} + F_{rvi} \qquad (6)$$

where $\dot{\beta}$ is the rotational speed of the flywheel. F_{jvi} and F_{rvi} are the inherent inertance and the friction force generated by the VI device.

By adjusting the damping of the PMSM, the equivalent inertance of the VI device becomes controllable in real-time. In the ideal scenario, with the PMSM damping set to zero, the flywheel freely rotates and remains disconnected from the ball screw. Conversely, when the PMSM damping is set to infinity, the flywheel behaves as if it is rigidly connected to the ball screw. Consequently, the output force of the VI device is dependent on the equivalent inertance of the flywheel and can be expressed as follows:

$$F_{vi} = rb\ddot{\beta} + F_{jvi} + F_{rvi} \qquad (7)$$

Thus, the dynamic model of the VI device can be built with the consideration of the flywheel:

$$C_{vi}(\dot{\alpha} - \dot{\beta}) = b\ddot{\beta} \qquad (8)$$

The damping generated by the PMSM can be controlled through varying the external resistance of the circuit. The controllable rotary damping of the PMSM is:

$$C_T = \frac{K_i K_e}{(R_e + R_i)} \tag{9}$$

where C_T is the real-time damping of the PMSM; K_i, R_i K_e are the voltage constant and current constant of PMSM. R_i, R_e are the internal resistance of PMSM, external resistance, respectively.

2.3 Mechanical Admittance Analysis

Admittance is the reciprocal of impedance. In this section, we establish the mechanical admittance in the frequency domain of the VIVD device. The analysis of mechanical admittance allows us to observe the variations in damping and inertance characteristics of the VIVD device and verify the validity of its topology. This section will focus on the controllability of the VIVD device with regard to damping and inertance. To facilitate controller design, we simplify uncontrollable forces, such as friction force and inertial friction of the shaft.

The mechanical admittance of VIVD device is:

$$Y_i = r^2 \left(C_{vd} + \frac{b^2 C_{vi} \omega^2}{b^2 \omega^2 + C_{vi}{}^2} \right) + \frac{r^2 b C_{vi}{}^2}{b^2 \omega^2 + C_{vi}{}^2} j\omega \tag{10}$$

Expressed in terms of resistance paraments as:

$$Y_i = r^2 \left(\frac{k^2}{R_i + R_{vd}} + \frac{b^2 k^2 \omega^2 (R_i + R_{vi})}{b^2 \omega^2 (R_i + R_{vi})^2 + k^4} \right) + \frac{r^2 b k^4 (R_i + R_{vi})^2}{(R_i + R_{vi})^2 b^2 \omega^2 + k^4} j\omega \tag{11}$$

where $k = K_i K_e$

The real part of the admittance represents the mechanical conductance and provides information about the equivalent damping. Besides, the imaginary part of the admittance corresponds to the mechanical susceptance, which carries information about the equivalent inertance. The equivalent damping and equivalent inertance are denoted as:

$$c_e = Y_{i(real)} = \frac{k^2}{R_i + R_{vd}} + \frac{b^2 k^2 \omega^2 (R_i + R_{vi})}{b^2 \omega^2 (R_i + R_{vi})^2 + k^4} \tag{12}$$

$$b_e = \frac{Y_{i(imag)}}{\omega} = \frac{r^2 b k^4 (R_i + R_{vi})^2}{(R_i + R_{vi})^2 b^2 \omega^2 + k^4} \tag{13}$$

Figure 3 illustrates that as the resistance decreases, both the mechanical conductance and the mechanical susceptance increase. With increasing frequency, the mechanical conductance continues to rise, whereas the mechanical susceptance initially increases, reaches a certain value, and then gradually decreases.

In Fig. 4, it can be observed that the equivalent damping and equivalent inertance of the VIVD device increase as the resistance of the external resistor decreases. Perform a detailed analysis of the frequency variations, Fig. 4 (a) reveals that the maximum

inertance of the VIVD device is 250 kg, and the equivalent inertance decreases with increasing frequency. On the other hand, Fig. 4 (b) demonstrates that the VIVD device exhibits different minimum damping values with varying external resistors, and the equivalent damping gradually increases with increasing frequency.
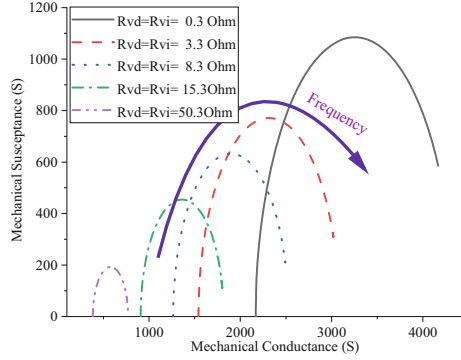
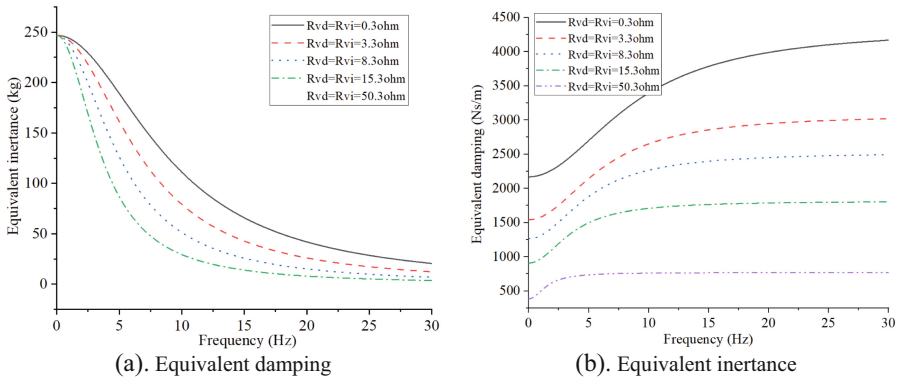

Fig. 3. The admittance of the VIVD device

(a). Equivalent damping

(b). Equivalent inertance

Fig. 4. Equivalent Mechanical properties of VIVD device

2.4   Parameter Identification

Figure 5 depicts a force-displacement test rig utilized for parameter identification. The designed VIVD device includes frictional forces that vary with velocity and inherent inertial forces that change with acceleration. Additionally, the parameters of the PMSM, such as current constants, voltage constants, and internal resistance, need to be identified. Friction and inertia forces are modeled as follows:

$$F_r = f_r sat\left(\dot{Z}_s - \dot{Z}_v\right) \tag{14}$$

$$F_j = r^2 J\left(\ddot{Z}_s - \ddot{Z}_v\right) \tag{15}$$

$$sat\left(\dot{Z}_s - \dot{Z}_v\right) = \begin{cases} 1\left(\dot{Z}_s - \dot{Z}_v\right) > \tau \\ (1/\tau)\left(\dot{Z}_s - \dot{Z}_v\right) - \tau \leq \left(\dot{Z}_s - \dot{Z}_v\right) \leq \tau \\ -1\left(\dot{Z}_s - \dot{Z}_v\right) < -\tau \end{cases} \tag{16}$$

Firstly, the excitation motion is $x = A\sin(2\pi ft)$, where $A = 0.01$ m, $f = 1.5$ Hz. The impact of external resistors on VIVD devices is verified by connecting resistors of varying values (50, 15, 8, 3, 0 Ω) to the circuit. Test results are shown in the. During VI device testing, the force generated by the VI device and the motion displacement exhibit negative stiffness characteristics, which increase as the resistance connected to the circuit decreases. The results indicate that adjusting the external resistance value of R_e can modify the inertance of the device. By analyzing the characteristic curves of VD devices, it is observed that the area of the enclosed curve increases as the external resistor R_e decreases, thereby indicating that the damping coefficient of both VD devices can be controlled by adjusting the external resistance R_e. The results demonstrate that the designed VIVD device possesses controllable inertance and damping. The controller can select suitable external resistors R_e to finely tune the damping and inertance of the seat suspension, thereby achieving effective seat control Figs. 5 and 6.
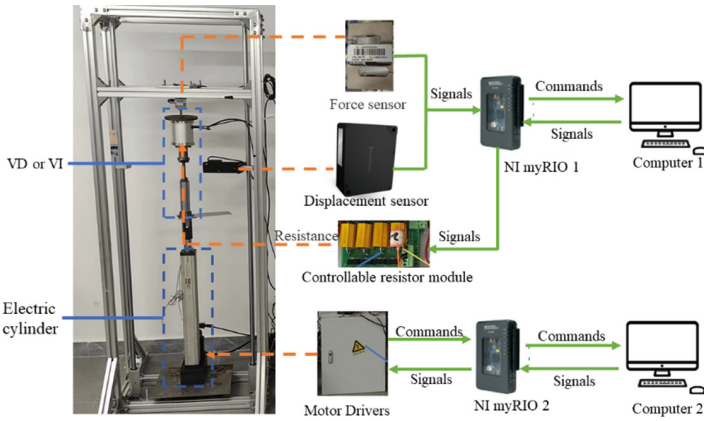
Fig. 5. Test platform

In the Figs. 7 and 8, different frequencies and amplitudes were set for the sinusoidal excitation to test the VI and VD devices respectively. When the frequency and amplitude increase, the area of the curved enclosure increases, which implies an increase in the output energy of the VIVD device. At the same time, the relative accuracy of the dynamic modelling of the VIVD device is verified by matching the experimental results with the simulation results under different operating conditions. Table 1 shows the results of the parameter identification.
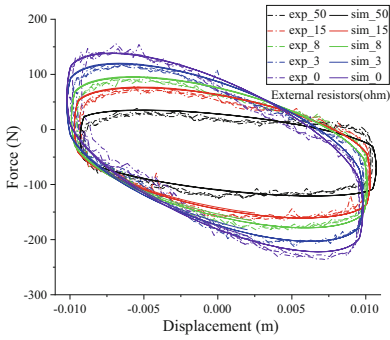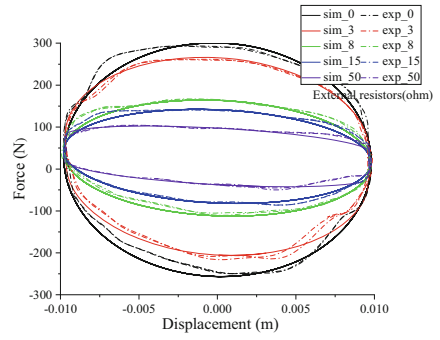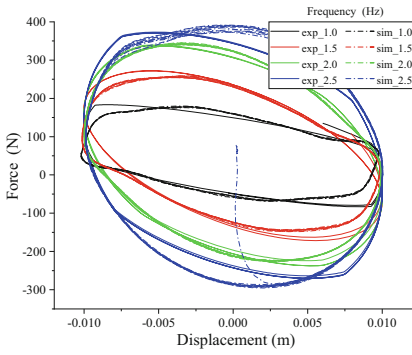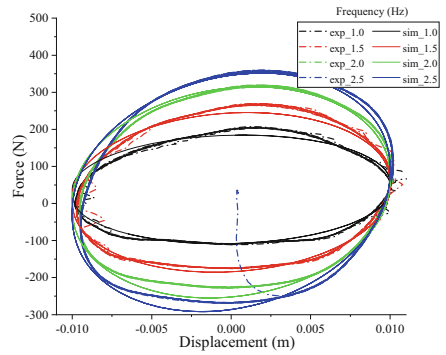
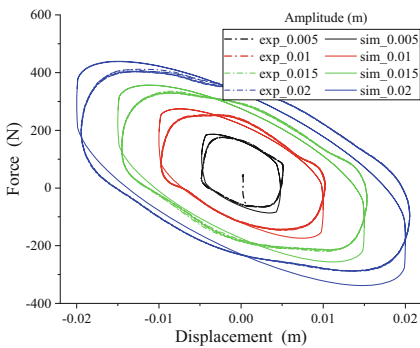**Fig. 6.** Characteristic curves of VIVD devices connected to different resistors

Fig. 7. Characteristic curves of VIVD devices under different frequency
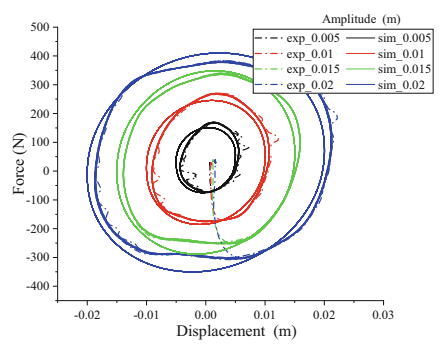
Fig. 8. Characteristic curves of VIVD devices under different amplitude

Table. 1. Parameter of VIVD device

Parameter	Symbol	Value
Coefficient of friction of VI device	f_{rvi}	35 N
Coefficient of friction of VD device	f_{rvd}	200×10^{-7} kgm^2
Inherent inertance of VI device	J_{vi}	30 N
Inherent inertance of VD device	J_{vd}	150×10^{-7} kgm^2
Moment of inertia of flywheel	b	160×10^{-5} kgm^2
Current constants (voltage constants) of PMSM	$K_i(K_e)$	0.41 Nm/s (Vs/rad)
Internal resistance of PMSM	R_i	10.5 Ohm

3   Controller Design

3.1   Adaptive Robust Sliding-Mode Controller

Ensuring the absolute accuracy of various parameters, such as friction and inertial forces, during the seat suspension design process is challenging. In this paper, we adopt the approach of attributing all uncertain characteristics to changes in the mass on the spring. This enables the controller to modify the seat suspension characteristics and adapt to changes in the dynamic characteristics of objects and perturbations. The uncertain dynamic characteristics model of the seat suspension can be described as:

$$M\ddot{Z}_s = -\Delta - f_{des} \tag{17}$$

$$\Delta = K(Z_s - Z_v) + F_r + F_j \tag{18}$$

where Δ is the disturbances and total uncertainty in the uncertainty component of the model, $u(t)$ is the desired dynamic output force of the VIVD device, M is the actual measurement of the mass on the spring.

The sliding surface is defined as:

$$s = \dot{e} + ce = \dot{Z}_s - \dot{Z}_d + ce \tag{19}$$

where Z_d is the desired displacement, which is assumed as zero. e is tracking error of the controller.

$$M\dot{s} = M(\ddot{Z}_s - \ddot{Z}_d + c\dot{e}) \tag{20}$$

Considering the Lyapunov functions as:

$$V = \frac{1}{2}Ms^2 + \frac{1}{2\gamma}\tilde{M}^2 \tag{21}$$

$$\tilde{M} = \widehat{M} - M \tag{22}$$

where $\widehat{M}$ is the estimated value of M.

So, its derivative is:

$$\dot{V} = Ms\dot{s} + \frac{1}{\gamma}\tilde{M}\dot{\tilde{M}} = s\big(M\ddot{Z}_s - M\ddot{Z}_d + Mc\dot{e}\big) + \frac{1}{\gamma}\tilde{M}\dot{\tilde{M}} \tag{23}$$

where $\gamma > 0$.

Substituting the formula (20):

$$\dot{V} = s\big(-\Delta - f_{des} - M\big(\ddot{Z}_d - Mc\dot{e}\big)\big) + \frac{1}{\gamma}\tilde{M}\dot{\tilde{M}} \tag{24}$$

Thus, the controller can be designed as:

$$f_{des} = -\widehat{M}\big(\ddot{Z}_d - Mc\dot{e}\big) + ks + \delta sign(s) \tag{25}$$

where δ should be greater than the upper limit of the perturbation,

$$\delta \geq \Delta_{max} \tag{26}$$

where Δ_{max} is the maximum values of Δ in the vehicle travelling.

Then,

$$\begin{aligned}
\dot{V} &= s\left(-\Delta - ks - sign(s) + \tilde{M}\big(\ddot{Z}_d - Mc\dot{e}\big)\right) + \frac{1}{\gamma}\tilde{M}\dot{\tilde{M}} \\
&= -ks - \delta \mid s \mid -\Delta s + \tilde{M}s\big(\ddot{Z}_d - Mc\dot{e}\big) + \frac{1}{\gamma}\tilde{M}\dot{\tilde{M}}
\end{aligned} \tag{27}$$

Adaptive law is designed to:

$$\dot{\widehat{M}} = -\gamma s\big(\ddot{Z}_d - Mc\dot{e}\big) \tag{28}$$

And,

$$\dot{V} = -ks^2 - \delta \mid s \mid -\Delta s \leq -ks^2 \leq 0 \tag{29}$$

If and only if $s = 0$, the $\dot{V} = 0$, the system is asymptotically stable. But when $\dot{V} = 0$, At this point V is no longer decreasing, therefore, there is no guarantee that $\tilde{M} \to 0$.

Thus, the design of the adaptive law should ensure that the value of The design of the adaptive law should ensure that the value of M lies between M lies between $[M_{min}, M_{max}]$,

$$M_{min} = \Delta_{min}/Z_{smax} + M \tag{30}$$

$$M_{max} = \Delta_{max}/Z_{smin} + M \tag{31}$$

The adaptive low is redesigned:

$$\dot{\widehat{M}} = Proj_{\widehat{M}}\big(-\gamma s\big(\ddot{Z}_d - Mc\dot{e}\big)\big) \tag{32}$$

$$Proj_{\widehat{M}}(\cdot) = \begin{cases} 0 & if\ \widehat{M} \geq M_{max}and\cdot > 0 \\ 0 & if\ \widehat{M} \leq M_{min}and\cdot < 0 \\ \cdot & otherwise \end{cases} \tag{33}$$

Besides the *sign(s)* is replaced by *sat(s)* in the implementation of the controller to suppress the chattering phenomenon in the sliding mode [16].

3.2 Force Tracking Controller

Due to the lack of external energy input, the VIVD device is unable to produce the desired force f_{des}. To address this, a force tracking controller based on energy priority storage (EPS) is designed in this section. The control scheme is display in the Fig. 9.

The sensors of seat suspension captured system status. Then, the upper layer ASMC controller calculated the f_{des}, the lower layer force tracking controller based on EPS calculated the output damping (C_{vi}, C_{vd}) of VIVD device. Eventually, the external resistance is selected to modify the mechanical characteristics of the seat suspension.

In the force tracking controller with EPS, the VI device is given the highest control priority to gather more energy for vibration attenuation. Meanwhile, the VD device is maintained at minimal damping, and the damping of the VI device changes in real-time while the flywheel collects the vibration energy.

$$C_{vd} = C_{min} \tag{34}$$

$$C_{vi} = (f_{des} - f_{vdmin})/\left(r^2(\dot{\alpha} - \dot{\beta})\right) \tag{35}$$

$$f_{vdmin} = rC_{min}\dot{\alpha} \tag{36}$$

where C_{min} and f_{vdmin} are the minimum value of damping and force of PMSM, respectively. The C_{vd} and C_{vi} are the damping of the VD and VI device, respectively.
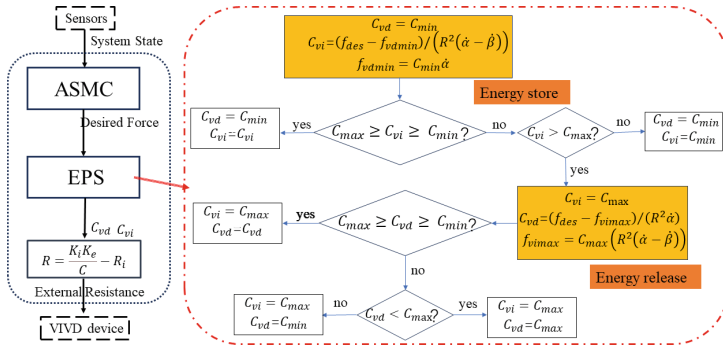

Fig. 9. Control scheme

When the $C_{vi} > C_{max}$, VD device enters the working state, energy stored in VI devices is released.

$$C_{vi} = C_{max} \tag{37}$$

$$C_{vd} = (f_{des} - f_{vimax})/\left(r^2\dot{\alpha}\right) \tag{38}$$

$$f_{vimax} = C_{max}r^2\left(\dot{\alpha} - \dot{\beta}\right) \tag{39}$$

where C_{max} and f_{vimax} are the maximum value of the damping and output force of the PMSM, respectively.

Finally, the right resistor is picked so that the PMSM produces the correct damping.

$$R_j = K_iK_e/C_j - R_ik \tag{40}$$

where R_j and C_j are the resistance value and damping of the VI and VD device, the j is the symbol of the VD or VD device.

4 Experimental System and Results Analysis

4.1 Experimental Setup

The experimental setup is shown in Fig. 10. The VIVD device is mounted on a quarter car suspension testing platform which is under the control of an NI myRIO; the vibration platform can generate desired vibration based on the commands from Computer 2. The relative displacement of the seat suspension is measured by a pulse type wire displacement sensor; and another wire sensor is applied to measure the displacement of the output displacement of the seat suspension. A force sensor is mounted under the VIVD seat suspension to measure the force of the VIVD seat suspension. A acceleration sensors are used to obtain the top accelerations of the seat suspension. An NI CompactRIO 9038 is used to control two controllable resistor based on sensors' feedback.

4.2 Vibration Control Test

In the random excitation, the characteristics of controller and vibration control performance of VIVD seat suspension are verified. A SM controller was designed, and a resistance of 8 Ω was connected to the circuit to make the VIVD seat suspension a passive suspension with fixed damping and inertance. These two types of suspension were used as comparison objects to verify the vibration control ability of ARSM control.
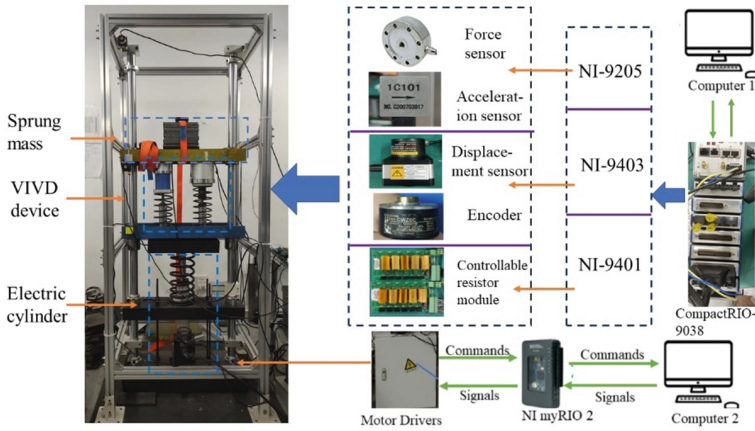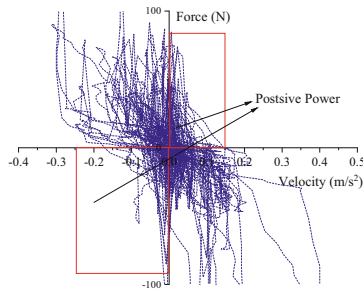
Fig. 10. Experimental setup.
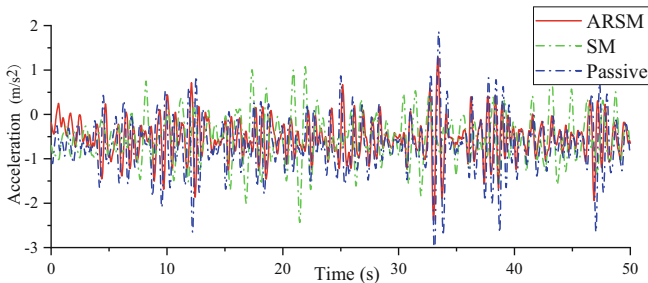

Fig. 11. Energy range

Fig. 12. Acceleration in the time domain

Figure 11 illustrates the energy output range of the VIVD seat suspension. It reveals that the VIVD seat suspension generates a positive output without any external energy input. This indicates that the flywheel can harvest vibration energy and utilize it to suppress the vibration. Figure 12 show the acceleration in the time domain, In the Fig. 12, the semi-active suspensions with ARSM controllers demonstrated reductions of 9.56%
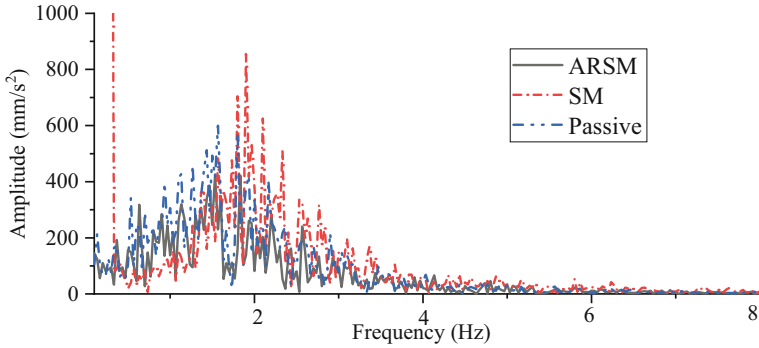
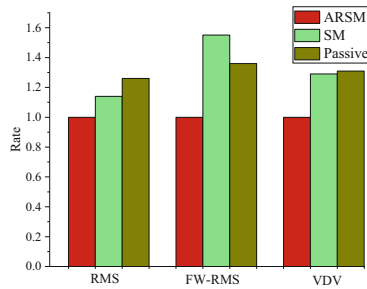**Fig. 13.** Acceleration in the frequency domain

Fig. 14. Parameters of vibration

and 21.89% in root-mean-square (RMS) acceleration compared with semi-active suspensions with SM controllers and passive seat suspension, respectively. Figure 13 shows the vibration absorption effect of the three seat suspensions in the frequency domain. When greater than 4 Hz, there is almost no difference in the vibration control ability of the three seat suspensions, but in the frequency range of 0.Hz-3 Hz, which is most perceptible to the human body, the semi-active seat suspension equipped with the ARSM controller exhibits the most significant mitigation effect. Figure 14 visualizes the vibration parameters, and the relative rates of the other two suspensions compared to the passive seat were calculated separately using the parameters of the passive seat suspension as a baseline.

5   Conclusion

In this study, the dynamic model of the VIVD seat suspension is determined firstly, and the topology of the VIVD device is established using the analysis method of mechanical admittance. Next, the prototype of the VIVD device is designed and manufactured, and its parameters are identified, the relevant parameters of the VIVD device are determined preliminarily. Following this, a two-layer control scheme is designed. An adaptive robust sliding mode controller is designed based on the traditional sliding-mode controller,

which corrects the error between the modelling process and the actual physical model through the adaptive adjustment of the structural parameters, Simultaneously, it enhances controller robustness and reduces the chattering phenomenon of sliding-mode control. The lower layer force tracking controller prioritizes the VI device for execution, ensuring efficient energy harvesting for vibration suppression by the VIVD device. Finally, the vibration control performance of both the conventional sliding mode control and the proposed ARSM controller is evaluated through traditional under random excitation. The ARSM control improves the vibration mitigation performance of the semi-active seat suspension by 9.56% using the same device, thus validating the effectiveness of the proposed control approach.

References

1. Kumar, S.: Vibration in operating heavy haul trucks in overburden mining. Appl. Ergonomics **35**(6), 509–520 (2004). https://doi.org/10.1016/j.apergo.2004.06.009
2. Liu, P., Ning, D., Luo, L., Zhang, N., Haiping, Du.: An electromagnetic variable inertance and damping seat suspension with controllable circuits. IEEE Trans. Ind. Electron. **69**(3), 2811–2821 (2022). https://doi.org/10.1109/TIE.2021.3066926
3. Le, T.D., Ahn, K.K.: A vibration isolation system in low frequency excitation region using negative stiffness structure for vehicle seat. J. Sound Vib. **330**(26), 6311–6335 (2011). https://doi.org/10.1016/j.jsv.2011.07.039
4. Yao, G.Z., Yap, F.F., Chen, G., Li, W.H., Yeo, S.H.: MR damper and its application for semi-active control of vehicle suspension system. Mechatronics **12**(7), 963–973 (2002). https://doi.org/10.1016/S0957-4158(01)00032-0
5. Ning, D., Sun, S., Zhang, J., Haiping, Du., Weihua, Xu., Wang, Li.: An active seat suspension design for vibration control of heavy-duty vehicles. J. Low Freq. Noise, Vib. Act. Control **35**(4), 264–278 (2016). https://doi.org/10.1177/0263092316676389
6. Sun, S.S., et al.: Horizontal vibration reduction of a seat suspension using negative changing stiffness magnetorheological elastomer isolators. Int. J. Veh. Des. **68**(1/2/3), 104 (2015). https://doi.org/10.1504/IJVD.2015.071076
7. Deng, L., et al.: Investigation of a seat suspension installed with compact variable stiffness and damping rotary magnetorheological dampers. Mech. Syst. Signal Process. **171**, 108802 (2022). https://doi.org/10.1016/j.ymssp.2022.108802
8. Ning, D., et al.: An electromagnetic variable inertance device for seat suspension vibration control. Mech. Syst. Signal Process. **133**, 106259 (2019). https://doi.org/10.1016/j.ymssp.2019.106259
9. Smith, M. C.: Synthesis of mechanical networks: the inerter, In: Proceedings of the 41st IEEE Conference on Decision and Control, 2002. 2002,
10. Smith, M.C., Wang, F.-C.: Performance benefits in passive vehicle suspensions employing inerters. Veh. Syst. Dyn. **42**(4), 235–257 (2004). https://doi.org/10.1080/00423110412331289871
11. Ning, D., et al.: A rotary variable admittance device and its application in vehicle seat suspension vibration control. J. Franklin Inst. **356**(14), 7873–7895 (2019). https://doi.org/10.1016/j.jfranklin.2019.04.015

12. Ning, D., Haiping, Du., Zhang, N., Jia, Z., Li, W., Wang, Y.: A semi-active variable equivalent stiffness and inertance device implemented by an electrical network. Mech. Syst. Signal Process. **156**, 107676 (2021). https://doi.org/10.1016/j.ymssp.2021.107676

13. Xiu-Mei, Du., Miao, Yu., Jie, Fu., Peng, Y.-X., Shi, H.-F., Zhang, H.: H∞ control for a semi-active scissors linkage seat suspension with magnetorheological damper. J. Intell. Mater. Syst. Struct. **30**(5), 708–721 (2018). https://doi.org/10.1177/1045389X18778340

14. Haiping, Du., James Lam, K.C., Cheung, W.L., Zhang, N.: Smart Mater. Struct. **22**(10), 105016 (2013). https://doi.org/10.1088/0964-1726/22/10/105016

15. Park, C., Jeon, D.: Semiactive vibration control of a smart seat with an MR fluid damper considering its time delay. J. Intell. Mater. Syst. Struct. **13**(7–8), 521–524 (2002). https://doi.org/10.1106/104538902030343

16. Hu, Y., Wang, K., Chen, M. Z. Q.: Semi-active suspensions with low-order mechanical admittances incorporating inerters, In: The 27th Chinese Control and Decision Conference (2015 CCDC), 2015, pp. 79–84

17. Li, Z., Zuo, L., Luhrs, G., Lin, L., Qin, Y.: Electromagnetic energy-harvesting shock absorbers: design, modeling, and road tests. IEEE Trans. Veh. Technol. **62**(3), 1065–1074 (2013). https://doi.org/10.1109/TVT.2012.2229308